Tailoring Ductile-Phase Toughened Tungsten Hierarchical Microstructures for Plasma-Facing Materials

Ba Nghiep Nguyen*, Charles H. Henager, Jr., Jing Wang, Wahyu Setyawan
Pacific Northwest National Laboratory, P.O. 999, Richland, WA 99352

Abstract: Biological materials, such as bones, nacre, etc., have been found to exhibit attractive and unique combinations of stiffness, strength and fracture toughness. Research has been conducted in various engineering areas to mimic the naturally hierarchical microstructures or nanostructures of these materials to produce materials with optimum stiffness, high strength and fracture toughness for their intended structural applications. In the same objective, this work applies a multiscale microstructural approach recently developed (*J. Nucl. Mater.*, (2018) 508: 371-384) to investigate the deformation and fracture behavior of ductile phase toughened tungsten (W) materials such as tungsten-nickel/iron (W-Ni/Fe) composites that possess lamellar-like and hierarchical "brick-and-mortar" (BAM) microstructures. First, the approach is used to simulate tensile loading of W-Ni/Fe specimens cut out from hot-rolled W-Ni/Fe plates which possess lamellar-like microstructures. The finite element model of the gage section of the specimen consists of a W-Ni/Fe dual-phase microstructural domain in which the constitutive behaviors of W and Ni/Fe phases are described by an elastic-plastic damage model. The predicted material stress-strain response and crack pattern development as a function of loading are then compared to the corresponding experimental results to determine the constitutive model parameters for W and Ni/Fe. Subsequently, the model parameters are used to analyze W-Ni/Fe BAM microstructures that are artificially created to investigate the effects of microstructural features and morphologies on the composite stress-strain response, damage, and fracture patterns. The modeling shows that regular BAM microstructures that experience bridging mechanism combined with crack penetration across W-phase regions exhibit significantly higher strengths than the rather random lamellar-like microstructures. More significantly, however adjusting the brick's length-to-height ratio, the BAM microstructure can be designed to allow a more distributed damage zone which leads to increased strength, ductility and fracture energy.

Keywords: Plasma-facing materials, hierarchical microstructure, ductile-phase toughening, damage modeling, finite element.

*Corresponding author: **Ba.Nguyen@pnnl.gov**

1. Introduction

Tungsten (W) alloys and W composites are currently the prime candidate materials for plasma-facing components (PFCs) of future fusion reactors such as the International Thermonuclear Experimental Reactor (ITER) and Demonstration Power Plant (DEMO). These W-based materials possess a high melting point, good strength at high temperatures, high thermal conductivity, low coefficient of thermal expansion, and low sputtering yields [1-3] that appear necessary for fusion energy applications. However, pure W and most W alloys can exhibit rather brittle behavior and suffers from high ductile-to-brittle transition temperatures. One way to mitigate the ductility issue is employing the concept of ductile-phase toughening (DPT), in which W brittle phase is embedded in a second ductile phase. Our previous results and report from other groups both confirmed significant improvement in DPT W composite materials [4-5].

In this paper we consider a variant of conventional DPT W composites, a hierarchical brick-and-mortar (BAM) composite, inspired by nature, where , biological materials such as nacre, teeth, shells, etc. have been found to exhibit attractive and unique combinations of stiffness, strength, and fracture toughness. Research has already been conducted in various engineering areas to mimic the kind of naturally occurring hierarchical microstructures or nanostructures of biological materials to produce materials with improved mechanical properties for their intended structural applications [6-8]. Gao [6] applied fracture mechanics concepts to hierarchical biomechanics of bone and bone-like materials to understand the nanoscale effect and mechanisms responsible for the optimized mechanical properties of these materials. This study indicates that understanding the mechanics or engineering principles in these naturally hierarchical materials may provide guidance to develop biologically inspired novel materials with unique properties. By exploring the features of the BAM structures found in enamel or nacre, Brandt et al. [7] proposed a multi-step processing procedure for hierarchical polymer composites by combining different coating techniques on different length scales. Henri and Pimenta [8] studied the damage tolerance that could be realized in a carbon-fiber polymer composite conceived as a hierarchical material by means of modeling and experiments. These authors found that the presence of discontinuities in the form of discontinuous fibers and hierarchical features promoted stable energy dissipation before failure. Combined, these microstructural features enabled disperse damage throughout the specimen leading to delays in damage localization that could otherwise occur in typically brittle composites.

Similar to these previous studies on other BAM materials, our work investigates the mechanical properties of ductile phase toughened (DPT) tungsten (W) composites that possess hierarchical BAM microstructures to elucidate the toughening mechanisms that are responsible for their mechanical properties in the hopes of further tailoring and improving them. To accomplish this, we examine the role of microstructural features and parameters that can contribute to the occurrence of a given or several toughening mechanisms and seek to understand the effect of the combined mechanisms on the composite stress-strain response. At the time of this paper, BAM materials have not yet been developed for high temperature applications such as PFCs for fusion energy applications. Particularly, no models exist that can guide the development of BAM materials for fusion energy science applications, although there have been general micromechanics-based models developed for these natural or synthetic materials that predict their mechanical properties including elastic stiffness, stress-strain response, fracture toughness etc. These models help understand the microstructural features, deformation and damage mechanisms that could lead to optimum combinations of mechanical properties [6-13]. Gorbatikh et al. [11] investigated in detail the failure mechanisms in hierarchical materials, including naturally occurring composites, and found that the structure of the reinforcement phase could change the failure initiation mechanism in a material with two levels of hierarchy by controlling the structure of the reinforcement phase on the lower level. More recently, Radi et al. [12-13] modeled BAM materials using direct element simulations and reported microcracking and crack deflection mechanisms that controlled strength, fracture toughness, and crack-growth toughness of these materials. In this work, we further elucidate these important mechanisms in our investigation of W-hierarchical composites relevant to fusion energy material application. Specifically, we apply a multiscale microstructural approach recently developed in [4] based on a W-copper (Cu) composite to investigate the tensile deformation and fracture behavior of DPT-W materials such as W-Ni/Fe composites that possess hierarchical lamellar-like and BAM microstructures. Previously, this approach was also successfully applied to simulate microcracking patterns and crack propagation in Ti_3SiC_2/SiC joints subjected to thermomechanical loading in addition to irradiation-induced swelling [14-15].

Our study does not focus on particular selection and qualification of W-Ni/Fe for PFMs. Research for testing W-Ni/Fe in fusion relevant conditions can be found in Refs [16-18]. The W-Ni/Fe composites have been adopted in this work primarily for the purposes of model

development, validation and illustration of the predictive capability needed to support the material design for PFCs. Predictive models that capture the toughening and damage mechanisms and their interactions are crucial to tailoring the mechanical properties to meet structural requirements for these applications. The same methodology for developing a predictive model of BAM W-NiFe composite as described in this work can then be applied to design other heavy W alloys of interest.

The use of Ni in fusion may raise a radiological concern. The plasma facing materials in divertor are expected to withstand the high heat flux and neutron irradiation doses in service for several years. The addition of Ni could lead to significant transmutation of Ni and production of helium, since Ni has a higher neutron interaction cross section than W and Fe in the relevant neutron spectrum [19]. Previous study to assess the activity of 97W-2.1Ni-0.9Fe composite (weight composition) under neutron irradiation condition at first wall of DEMO shows that the activity of the 97W with 5 years of service is very similar to that of pure W after 1 year cooldown, and it is less than two times higher than pure W after 10,000 years [16]. Another study advises that the limitation of Ni is 10 at.% to qualify as a class C waste [20-21]. All these studies suggest that W-Ni/Fe composites containing a few percentages of Ni are acceptable for fusion application. Nevertheless, further neutronics studies are clearly needed to assess the overall volume limit of Ni based on the designs of the fusion devices. Such studies are beyond the scope of this work.

The structure of this paper is as follows. Section 1 provides an introduction. Section 2 describes the microstructural approach [4] involving finite element (FE) discretization of the microstructure and constitutive modeling. This section then describes the application of the modeling approach to simulate tensile loading of W-Ni/Fe specimens cut out from hot-rolled W-Ni/Fe plaques. The predicted material stress-strain response and crack pattern development as a function of loading are then compared to the corresponding experimental results to determine the constitutive model parameters for W and Ni/Fe. Section 3 describes the design of BAM microstructure to achieve improved mechanical properties using the constitutive model parameters obtained in Section 2. Then, Section 3 discusses the effects of microstructural parameters on the damage and crack development that affect mechanical properties of BAM composites. Section 4 draws conclusions from this work.

2. Multiscale microstructural modeling

2.1 Finite element discretization of the microstructure

We investigate the deformation behavior of ductile phase toughened W materials such as W-Ni/Fe composites using the Nguyen et al.'s multiscale microstructural approach [4] that involves a dual-phase model where the two constituent phases (i.e., W and Ni/Fe) are finely discretized in finite elements (FEs) and described by a continuum damage mechanics (CDM) model. This approach is suitable for modeling deformation, cracking, and crack bridging for W-Ni/Fe, and other ductile phase toughened W-composites, or more generally, any multi-phase composite structure where two or more phases undergo cooperative deformation in a composite system.

The hot-rolled W-Ni/Fe material (weight composition of 90W-7Ni-3Fe) studied and defined as the baseline material in this work has a lamellar-like microstructure as presented in Fig. 1a. The image shown in Fig. 1a corresponds to a central part of a W-Ni/Fe tensile specimen located on the specimen's symmetry axes away from the gripped ends. This part is 0.584-mm long, 0.584-mm wide and 0.25-mm thick. It belongs to the specimen portion of interest that does not include the entailed sections and is 5-mm long, and 1.168-mm wide. The nominal W volume fraction in the composite is about 0.8. To construct a 3D model from a 2D image, the 2D image is simply extended in the thickness direction (out-of-plane) to form a uniform microstructure along this direction. Since the specimen was subjected to a uniform tensile loading, only a representative domain located on the symmetry axes which covered half of the specimen width was modeled.

The discretization of the 2D finite elements was achieved based on a digital image using the OOF2[1] software. The 2D FE model with boundary conditions illustrated in Fig. 1b contains the dual-phase W-Ni/Fe microstructural domain created using the Nguyen et al. method [4] that captures the constitutive behaviors of W and of the Ni/Fe alloy described by an elastic-plastic damage model. Although OOF2 can capture the actual microstructure obtained with SEM at some level of details, information such as chemical, compositional variations, impurities, and dislocation, etc. are not included. The model assumes composition and other factors are uniform within each phase boundary. Since the modeling domain is located on the specimen's symmetry axes, the corresponding displacements along the *x*- and *y*-directions on the domain left and bottom boundaries are fixed, respectively, while a uniform displacement parallel to the *x*-direction is applied on the domain right boundary (Fig. 1b). A magnified view of a local region inside the domain is given in Fig. 1c showing the detailed mesh.

[1]Software developed at the National Institute of Standards and Technology.

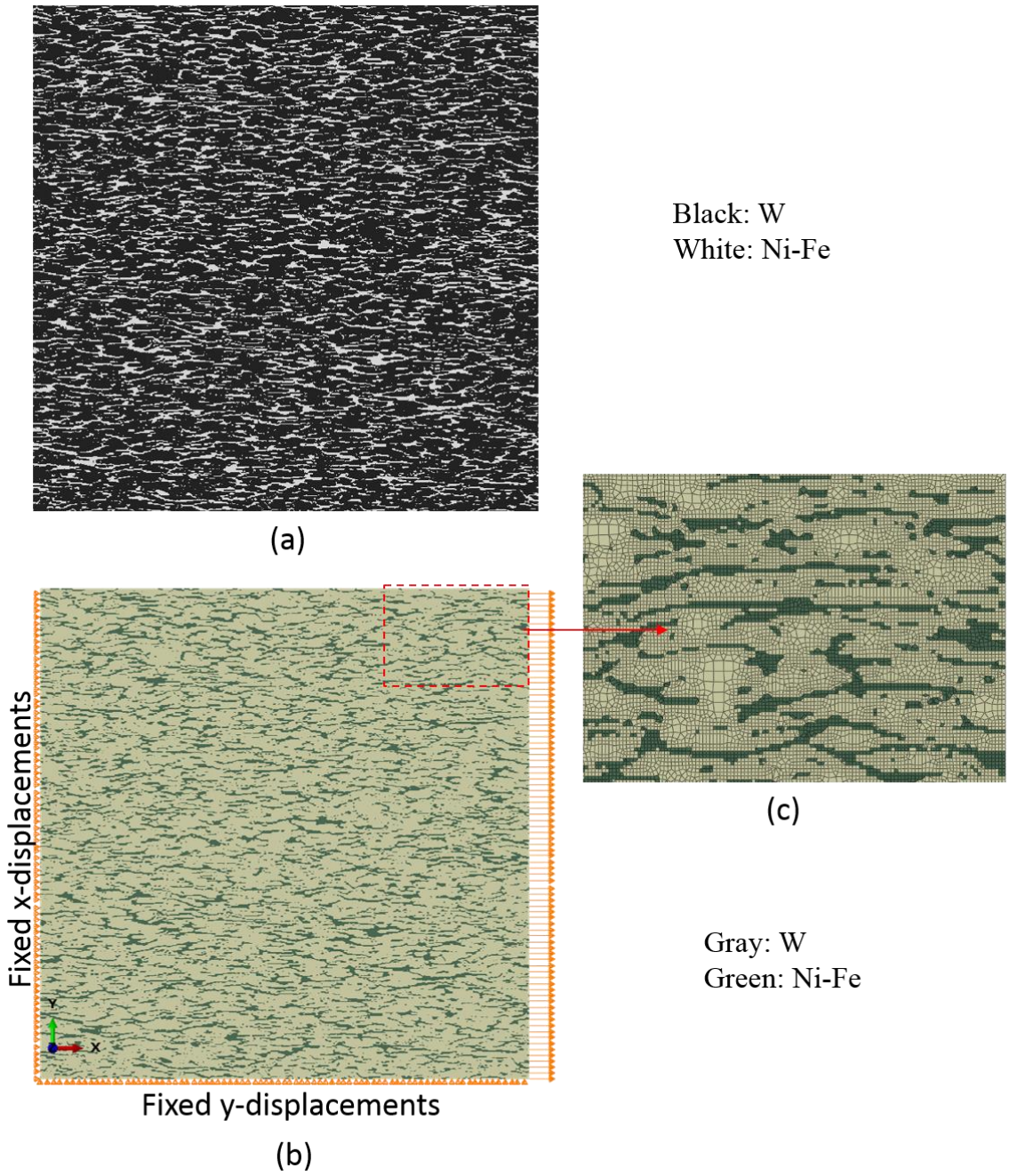

Figure 1. (a) The digital image of the as-formed dual-phase microstructure from a tensile specimen, (b) The associated FE model with boundary conditions for analysis, and (c) a magnified view showing the mesh details.

2.2 Constitutive relations

The constitutive responses of W and Ni/Fe in the dual-phase region are described by a CDM formulation previously used [4]. The model uses the J_2 deformation theory of plasticity and the

158 principle of strain equivalence (Lemaitre [22]) which states that the elastic or plastic constitutive
159 equations of a damaged material derived from the same formalism as the virgin material by
160 expressing these equations in terms of the effective stress tensor as:

$$\tilde{\sigma}_{ij} = \frac{\sigma_{ij}}{1-D} \tag{1}$$

161 where σ_{ij} is the stress tensor and D is the isotropic damage variable.

162 The modified Ramberg-Osgood relation (Nguyen and Kunc [23]) that describes the material
163 nonlinear stress-strain response affected by damage is expressed in terms of the equivalent
164 effective stress as:

$$\bar{\varepsilon} = \frac{\bar{\sigma}}{E\,(1-D)} + \frac{\sigma_0}{E}\left(\frac{\bar{\sigma}}{\sigma_0(1-D)}\right)^n = \frac{\bar{\tilde{\sigma}}}{E} + h\,\bar{\tilde{\sigma}}^n \tag{2}$$

165 where $\bar{\varepsilon}$, $\bar{\sigma}$, and σ_0 are the total equivalent strain, equivalent stress and reference stress,
166 respectively. The first and second terms of the right-hand side of Eq. (2) represent the equivalent
167 elastic and plastic strains, respectively. The coefficient h is given by $h = \sigma_0^{1-n}/E$ where E and n are
168 the elastic modulus of the undamaged material and power-law exponent. The "tilde" symbol
169 denotes an effective quantity based on the principle of strain equivalence as in Eq. (1). For an
170 elastic-plastic material without consideration of damage, the modified Ramberg-Osgood relation
171 (Eq. 2) reduces to the well-known Ramberg-Osgood relation (Ramberg and Osgood, 1943) [24].
172 In Eq. (2), the equivalent stress is expressed as a function of the equivalent plastic strain, $\bar{\varepsilon}^{\mathrm{p}}$:

$$\bar{\varepsilon}^{\mathrm{p}} = h\left(\frac{\bar{\sigma}}{1-D}\right)^n \tag{3}$$

$$\bar{\sigma} = (1-D)\,k\,(\bar{\varepsilon}^{\mathrm{p}})^{1/n} \tag{4}$$

173 where $k = (1/h)^{1/n}$ is the hardening coefficient. Next, in the framework of the deformation theory
174 of plasticity and considering proportional loading, the Lemaitre-Chaboche damage evolution law
175 for isotropic hardening materials (Lemaitre and Chaboche, [25]) is used to express the damage
176 variable increment in terms of the equivalent plastic strain increment:

$$dD = \frac{D_c}{\bar{\varepsilon}_p^R - \bar{\varepsilon}_p^D}\left(\left[\frac{2}{3}(1+\nu) + 3(1-2\nu)\left(\frac{\sigma^h}{\bar{\sigma}}\right)^2\right] d\bar{\varepsilon}^p\right) \quad (5)$$

where $\bar{\varepsilon}_p^D$ and $\bar{\varepsilon}_p^R$ are the equivalent plastic strains at damage initiation and at rupture, respectively, and D_c is the value of D at rupture, ν is Poisson's ratio, and σ^h the hydrostatic stress. The effective stress increment is related to the total strain increment by the constitutive equation:

$$d\tilde{\sigma}_{ij} = C_{ijkl}(D)d\varepsilon_{kl} \quad (6)$$

where the material tangent stiffness tensor $C_{ijkl}(D)$ reflects both plasticity and damage.

Damage evolves with deformation according to the damage evolution law Eq. (5) until a critical (saturation) state occurs for which $D = D_c$ $(0 < D_c \leq 1)$ and failure results. In the current model, damage is not activated under a compressive state of stress, rather the material is modeled as elastic-plastic and obeys a classical Ramberg-Osgood relation [24] under compression. The occurrence of failure implies that the failed material at a given location can no longer carry loads. In this work, failure at damage saturation leading to crack initiation and propagation is modeled by a vanishing finite element method [26, 4]. This damage model has been implemented in the Abaqus FE package. The detailed of the computational procedure is given in Nguyen et al. [4].

2.3 Analysis results for the baseline W-Ni/Fe microstructure

The 2D plane-stress model (Fig. 1b) of the W-Ni/Fe specimen subjected to tensile loading was analyzed using Abaqus and the elastic-plastic damage model described in the previous section to depict the constitutive behaviors of W and Ni/Fe phases in the microstructural domain. A series of FE analyses was first conducted to determine the constitutive parameters for the damage model. Typical constitutive parameters of W and of Ni alloys were used as the initial guesses. However, since the actual properties of the two phases are not known, the constitutive parameters are adjusted through FE analyses until the predicted stress-strain response and loading-dependent damage pattern development reasonably agree with the corresponding experimental results. Fig. 2a shows the predicted engineering stress-strain response that agrees well with the corresponding experimental data (also plotted on this figure). The damage model parameters for W and Ni/Fe determined through these analyses are given in Table 1 and it should be noted that the fitted

parameters are reasonable for both W and Ni/Fe phases. In the next section, these parameters are used as constitutive material inputs for W and Ni/Fe in BAM microstructural models for studying the hierarchical microstructure effect on the stress-strain response of the as-designed BAM composite.

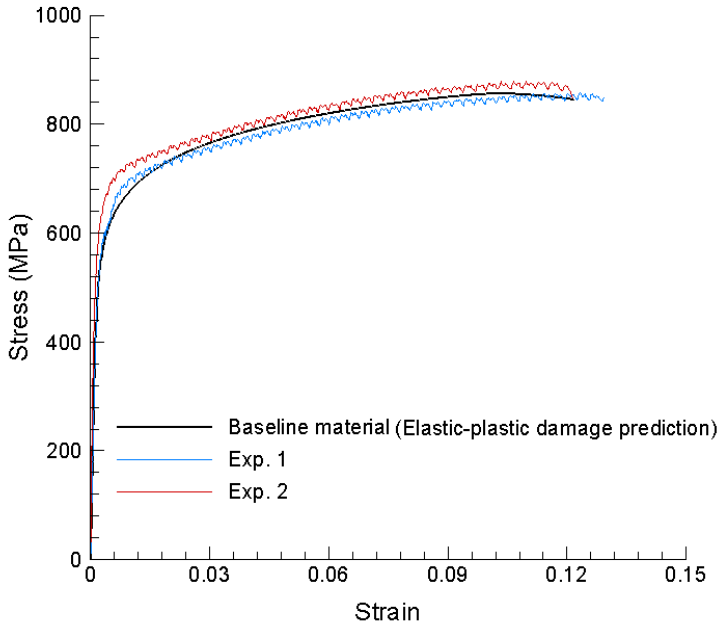

Figure 2. Predicted true tensile stress-strain response for the baseline W-Ni/Fe composite compared to the corresponding experimental data obtained using digital image correlation (DIC) data from the tensile gage section of miniature tensile specimens described in Section 2.l.

Table 1. Parameters of the elastic-plastic damage model for W and Ni/Fe in the dual-phase microstructural domain.

Material	E (MPa)	v	σ_0 (MPa)	n	$\bar{\varepsilon}_p^D$	$\bar{\varepsilon}_p^R$	D_c
Ni/Fe	203570	0.304	250	7	0.2	0.65	0.98
W	383000	0.28	760	12.5	0.25	0.5	0.98

Figs 3a and 3c illustrate the predicted damage distributions and crack patterns at 0.04 and 0.12 overall strains, respectively. At 0.04 strain, significant damage has been predicted to accumulate in the composite. At this loading level, damage has preferentially developed inside the Ni/Fe regions. However, at 0.12 strain that corresponds to about the elongation limit, many macrocracks were formed by the linking-up of failed Ni/Fe and W elements. The predicted damage and crack patterns reasonably agree with the experimental observations illustrated in Figs. 3b and 3d that show the SEM images of a tested sample region at 0.04 and 0.125 overall strains, respectively. Figs 4(a-d) illustrate in detail the occurrence of damage mechanisms as a function of loading. Fig. 4a shows a magnified view of a sub-domain inside the modeling domain where the areas colored in gray and green depict the W and Ni-Fe phases, respectively. Fig. 4a is used to identify the regions for damage and fracture occurrences. At 0.04 applied strain (Fig. 4b), damage has already initiated in some Ni/Fe regions since a number of Ni/Fe elements have experienced nonzero to relatively high values of the failure indicator in these regions. At 0.085 strain these Ni/Fe elements start failing (failure indicator = 1) and microcracks are formed by the linking-up of failed Ni/Fe elements as clearly shown in Fig. 4c. Figs 4b and 4c illustrate the DPT mechanism caused by damage and failure of the ductile Ni/Fe elements between W elements. When the applied strain is increased to 0.12, the microcracks are also able to penetrate the W regions causing the W elements to fail. The linking-up of microcracks through both W and Ni/Fe regions forms a visible macrocrack shown in Fig. 4d at this loading level that triggers a combination of two failure mechanisms: the DPT and the fracture of W mechanisms. Fig. 4e shows an SEM of a local crack that propagated through W regions adjacent to Ni/Fe regions and appears similar to the predicted crack paths in Fig. 4d.

The agreement between predicted and experimental crack development results can only be qualitative due to the following reasons. First, due to the statistical nature of the microstructure, the microstructure used to develop the FE model of the dual-phase domain for the tensile specimen was not identical to the one from the tested specimen. We can see clearly on Fig. 4a compared to Fig. 4e that the FE model microstructure contains a weak path (involving many Ni/Fe elements) that favored crack propagation along this path while the tested specimen microstructure does not have such a path or the same path. Second, the experimental crack patterns at two different deformation levels were captured at a specimen's surface. Three-dimensional crack patterns might reveal more complex microcrack distributions and higher crack density closer to the predicted

crack patterns; and third, the 2D FE model could overpredict damage and crack development. Third, the FE model does not contain the W-W grain boundaries that are present in the microstructure. Finally, the current model does not consider effects such as compositional variations and impurities that influence on the mechanical properties. The influence of composition variation and impurity can only be incorporated in the FE model through the composition and impurity dependence of the constitutive behaviors. However, such input information is currently unavailable and more detailed and accurate experimental measurements are needed in the future to improve the model.

However, in addition to the DPT mechanism, we have identified two other important toughening mechanisms, namely distributed damage zone over the dual-phase domain and crack penetration across the W phases at high loading levels. The multiplication and distribution of microcracks that develop over a large area of the dual-phase domain (as shown in Fig. 3) correspond to increased strength and ductility when the applied deformation is increased from 0.04 to ~0.12 (as shown Fig. 2).

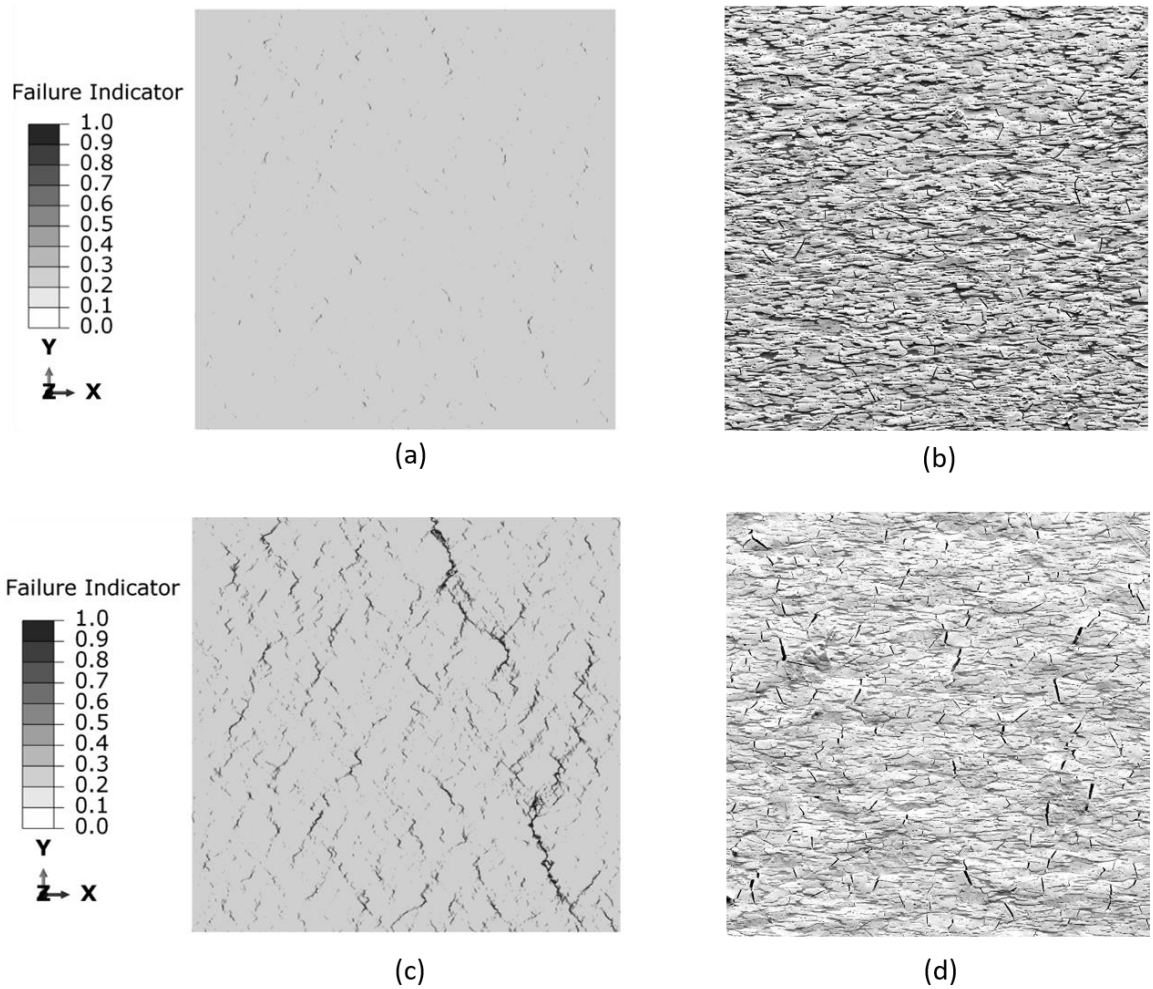

Figure 3. Predicted damage distribution and fracture patterns at (a) 0.04 and (b) 0.12 overall strains. Optical images of surface cracks on experimental tensile specimens strained to (c) 0.04 and (d) 0.125 overall strains.

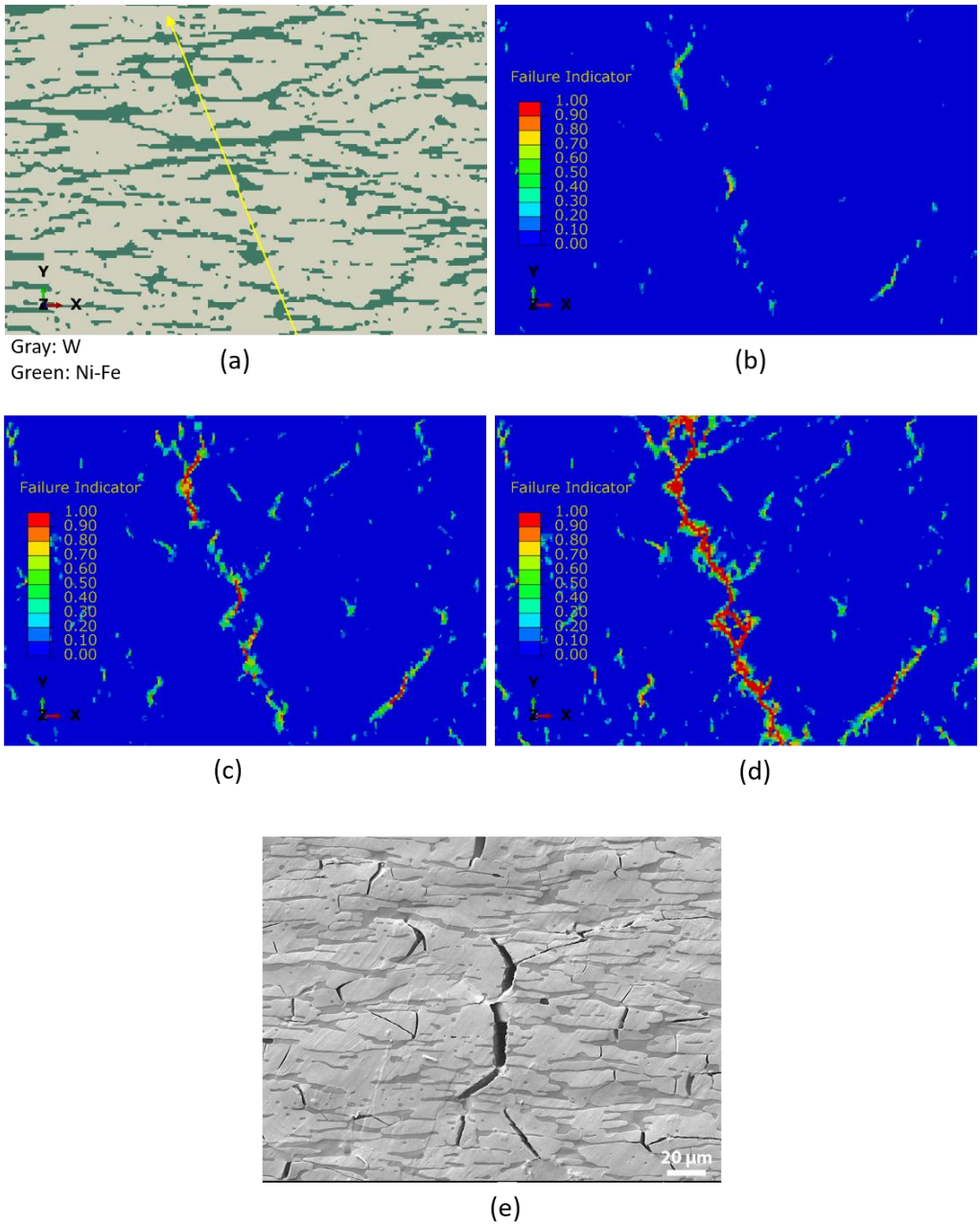

Figure 4. (a) A magnified view of a local area inside the microstructural domain (yellow arrow indicating a preexisting weak path favoring crack propagation), (b) Predicted local damage distribution at 0.04 strain, (c) Predicted local damage distribution and crack propagation at 0.085 strain, (c) Predicted cracks formed by the linking-up of failed Ni-Fe and W elements at 0.12 strain, and (e) SEM image of cracks near the fracture path in the tensile sample strained to failure.

3. Tailoring W-Ni/Fe microstructure for improved mechanical properties

3.1 "Brick-and-mortar" microstructures

Hierarchical "brick-and-mortar" (BAM) microstructures have been shown to be able to combine high stiffness, strength and fracture toughness [6-13]. In this section, a series of regular W-Ni/Fe BAM microstructures are generated to evaluate the potential of such microstructures to achieve improve strength, ductility and fracture energy in comparison to the baseline lamellar-like microstructure analyzed in the previous section. Various BAM microstructures can be generated by varying key microstructural features such as brick's volume faction, length, height, width, length-to-height aspect ratio *L/H*, brick's spacing and relative positions, etc. In this work, for the sake of the modeling approach illustration and meaningful comparisons with the baseline microstructure in terms of W content, microcrack distributions and their effects on the BAM composite's mechanical properties, all the generated BAM microstructural domains contain the same volume fraction of W (0.8) and have the same dimensions (0.584 x 0.584 x 0.025 mm) as the baseline microstructure. In addition, they have the same topology in terms of bricks' relative positions from one to another. These considerations are the constraints of our problem that aims at tailoring the BAM microstructure by varying the aspect ratio *L/H* in order to maximize the fracture energy.

Fig. 5 shows an example of a BAM microstructure having two hierarchical levels: Level 0 corresponds to a single W "brick" with length *L* and height *H*; Level 1 includes the representative W-brick-and-Ni/Fe "mortar" unit cell that is repeated in both horizontal (x) and vertical (y) direction to build the microstructural domain. The thickness *t* of the Ni/Fe mortar is adjusted such that the W volume fraction is kept at 0.8 for the modeling domain. Figs 6(b-f) show the as-generated BAM microstructures with *L/H* = 5, 10, 20, 30 and 40, and Fig. 6a presents the baseline lamellar-like microstructure for a comparison with the BAM ones.

3.2 Elastic modulus computation

First, we studied the evolution of the elastic modulus of the BAM microstructures in the reinforcement direction of interest which is the *x*-direction along the brick length. To this end, the BAM microstructures were discretized in 2D finite elements (about 250000 elements) working under plane-stress or plane-strain assumptions subject to similar boundary conditions to those illustrated in Fig. 1b for the baseline microstructure. Figs 7a and 7b respectively report the plane-

strain and plane-stress FE solutions for the normalized composite elastic modulus, E^{c}_{xx}/E_{b} (E_{b} being the W brick elastic modulus) as a function of the brick aspect ratio *L/H* for the prescribed values of the constituent modulus ratio, $E_{m}/f_{m}E_{b}$. Since the brick modulus (i.e., E_{b}= 383 GPa) and the brick volume fraction (f_{b}= 0.8) are given, the mortar elastic modulus, E_{m} is determined from the modulus ratio and $f_{m} = 1 - f_{b}$. For a W-Ni/Fe composite studied in this paper or a W-Cu composite with the same W volume fraction and known constituent elastic modulus, the modulus ratios are 2.66 and 1.44, respectively. Figs 7a and 7b show that if the ratio, $E_{m}/f_{m}E_{b}$ is small (<< 1), the composite modulus increases substantially with the increasing brick aspect ratio *L/H* and tends to saturate for large aspect ratios (> 90). In fact, the limit or saturation of the composite elastic modulus for the inclusion aspect ratio tending toward infinite is a known problem in composite materials. For larger and larger values of $E_{m}/f_{m}E_{b}$, the effect of *L/H* is smaller and smaller and becomes negligible for the W-Ni/Fe composite.

The plane-strain FE solutions agree very well with the numerical predictions by an Eshelby-Mori-Tanaka approach (EMTA [27-29]) only for small modulus ratios (< 0.1), while the plane-stress FE results agree globally well with the EMTA predictions for all constituent modulus ratios considered including the values for the W-Ni/Fe and W-Cu composites. In the EMTA computation, ellipsoidal brick inclusions were assumed. To further investigate the elastic modulus computations, our FE plane-strain results and EMTA solutions presented in Fig. 7a are compared to the Begley et al.'s plane-strain micromechanical solutions [7] for the same modulus ratios (0.02, 0.05 and 0.1). It is seen in Fig. 8 that Begley et al.'s results agree fairly well with the FE solutions for small to moderate brick aspect ratios (*L/H* < 20), but the results diverge for larger brick aspect ratios. The same findings are found when comparing EMTA's solutions to Begley et al.'s results. In fact, the modulus saturation for large brick aspect ratios is not realized in Begley et al.'s model, and that explains the significant divergence of our solutions compared to Begley et al.'s for large brick aspect ratios.

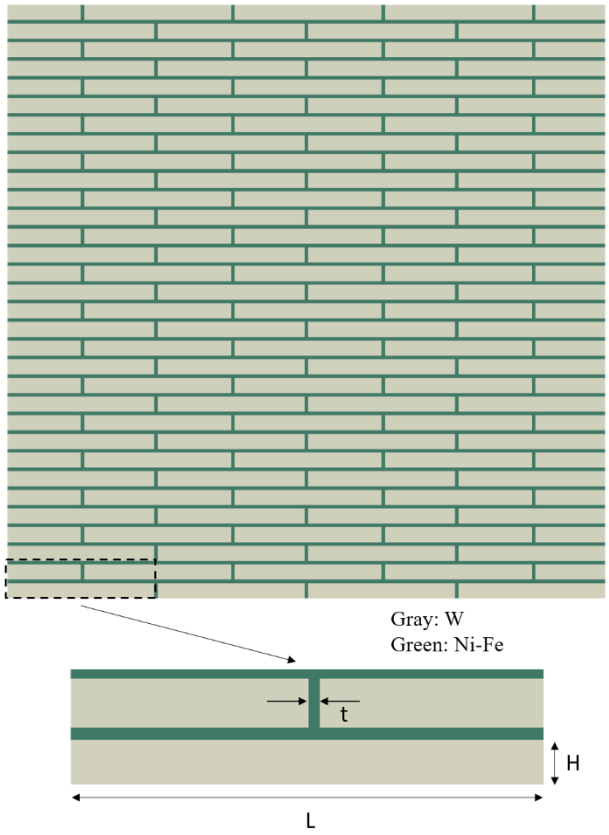

Figure 5. An example of BAM microstructure for W/Ni-Fe showing two hierarchical levels: Level 0 corresponds to a single W "brick" with length *L* and height *H*; Level 1 includes the representative W-brick-and-Ni/Fe "mortar" unit cell that is repeated in both horizontal (x) and vertical (y) direction to build the microstructural domain.

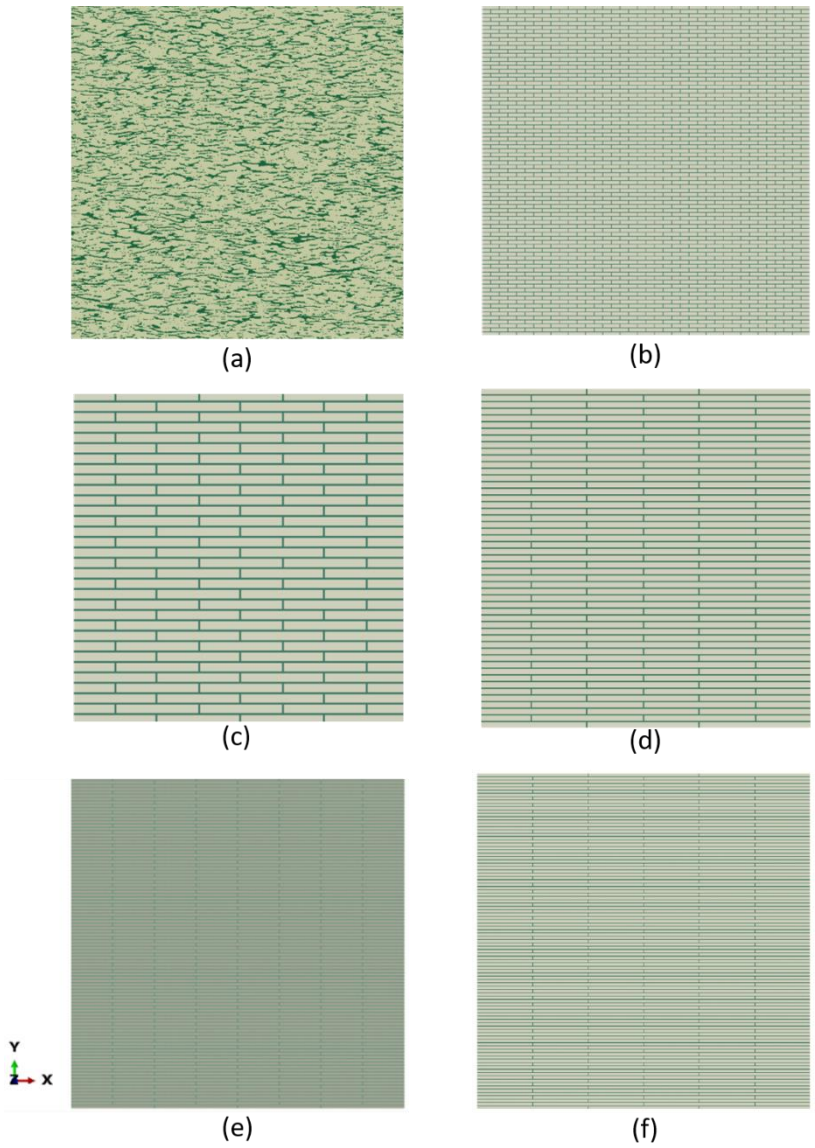

Figure 6. (a) Baseline lamellar-like microstructure - Generated BAM W/Ni-Fe microstructures (gray: W, green:Ni/Fe): (b) *L/H*=5, (c) *L/H*=10, (d) *L/H*=20, (e) *L/H*=30, and (f) *L/H*=40.

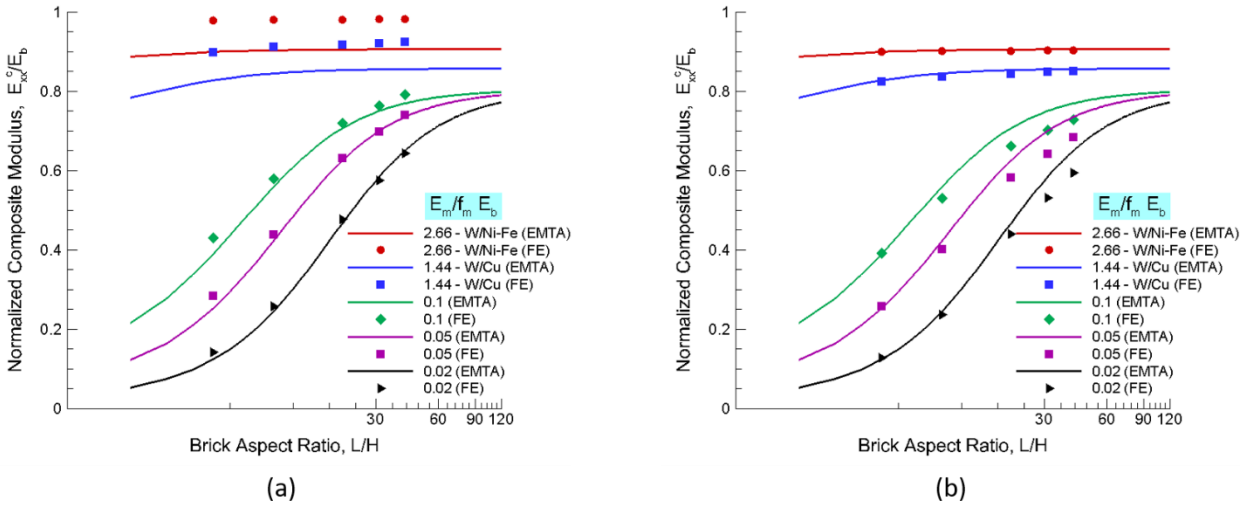

Figure 7. Normalized composite modulus as a function of the brick aspect ratio: (a) Plane-strain FE and (b) Plane-stress FE results compared to EMTA solutions.

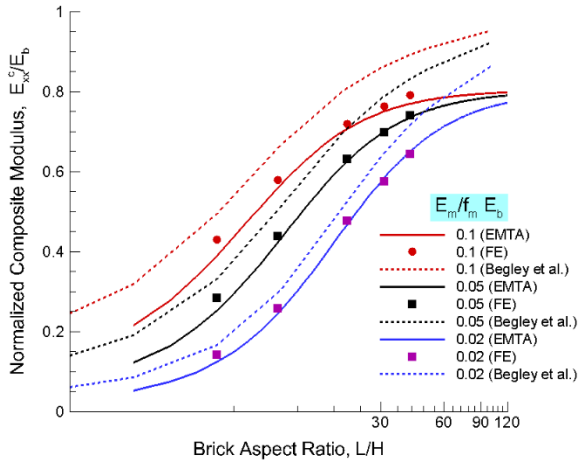

Figure 8. Normalized composite modulus as a function of the brick aspect ratio: plane-strain FE results and EMTA predictions compared to Begley et al.'s results [7].

3.2 *Stress-strain response and damage predictions*

A series of FE analyses of the BAM models illustrated in Fig. 6 was conducted to compare the mechanical performance of the BAM microstructures in terms of the overall stress-strain response to that of the actual hot-rolled microstructure (Fig. 6a). The model parameters given in Table 1

were used for W and Ni/Fe in all the FE analyses of the BAM microstructural models to investigate the W brick aspect ratio and microstructural effects on the stress-strain behavior, damage and crack development in these composites. Fig. 9 reports the stress-strain curves up to failure of these composites compared to the predicted response of the baseline composite shown in Fig. 2. The results on this figure show that increasing the brick aspect ratio *L/H* from 10 to 40 results in a significant increase in strength but a reduction in fracture strain. In addition, strength saturation with increasing *L/H* from *L/H* = 30 has been found. For small brick aspect ratios such as the case for *L/H*=5 illustrated in Fig. 6b, the model predicts a significant increase in strength combined with an important increase in fracture strain. Table 2 gives the predicted strengths and fracture strains for all the cases. The fracture strains correspond to the strains at the maximum stresses (strength) on the stress-strain responses presented in Fig. 9. It is seen in this table that *under the prescribed constraints and selected design parameters for our microstructural tailoring problem*, the BAM with *L/H*=40 possesses the highest strength (889 MPa) but the lowest fracture strain (0.0848) while the BAM which *L*/*H*=5 appears to have an optimum solution with a high strength (880.4 MPa) and the highest fracture strain (0.1737).

Table 2. Predicted strengths and fracture strains for the BAM microstructures compared to the predicted and experimental results for the baseline hot-rolled microstructure.

Microstructure	**Strength (MPa)**	**Fracture Strain**
Hot-rolled (predicted)	856.6	0.1064
Hot-rolled (experimental*)	867.8	0.112
BAM (*L/H* = 5)	880.4	0.1737
BAM (*L/H* = 10)	863.	0.1054
BAM (*L/H* = 20)	881.2	0.0954
BAM (*L/H* = 30)	887.3	0.0904
BAM (*L/H* = 40)	889.	0.0848

(*) Average values from two experiments

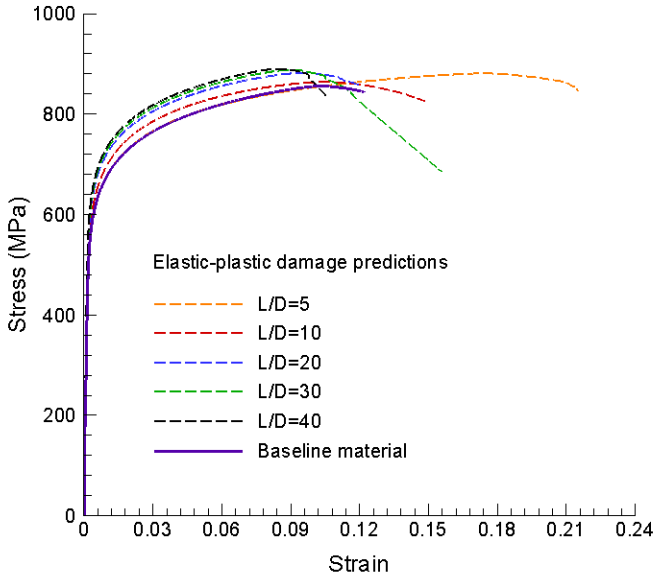

Figure 9. Predicted tensile stress-strain responses for the BAM composites shown in Figs 6(b-f) compared to the predicted response for the baseline material (Fig. 6a).

The damage and fracture patterns for all the cases presented in Figs 10(a-f) elucidate the stress-strain responses in Fig. 9. For comparison, Fig. 10a shows the results for the baseline hot-rolled material already discussed in Section 2. Figs 10(b-f) illustrate the damage and fracture patterns in the BAM microstructures with aspect ratios 5, 10, 20, 30 and 40, respectively. As previously mentioned, in addition to the *DPT mechanism* caused by failed Ni/Fe elements, there are two other mechanisms found: *crack penetration across tungsten phase* and *multiplication of cracks* over the domain. More importantly these mechanisms combined occur during loading, more facture energy is dissipated leading to higher strength and fracture strain. This is realized with the L/H = 5 BAM microstructure. The fracture patterns in the other BAM microstructures (with L/H = 10, 20, 30, 40) are quite similar: increasing L/H has led to increased strength. More damage distributed in the L/H=10 BAM has yielded higher fracture strain for this case. All the BAM materials exhibit higher strength than the baseline composite's predicted strength.

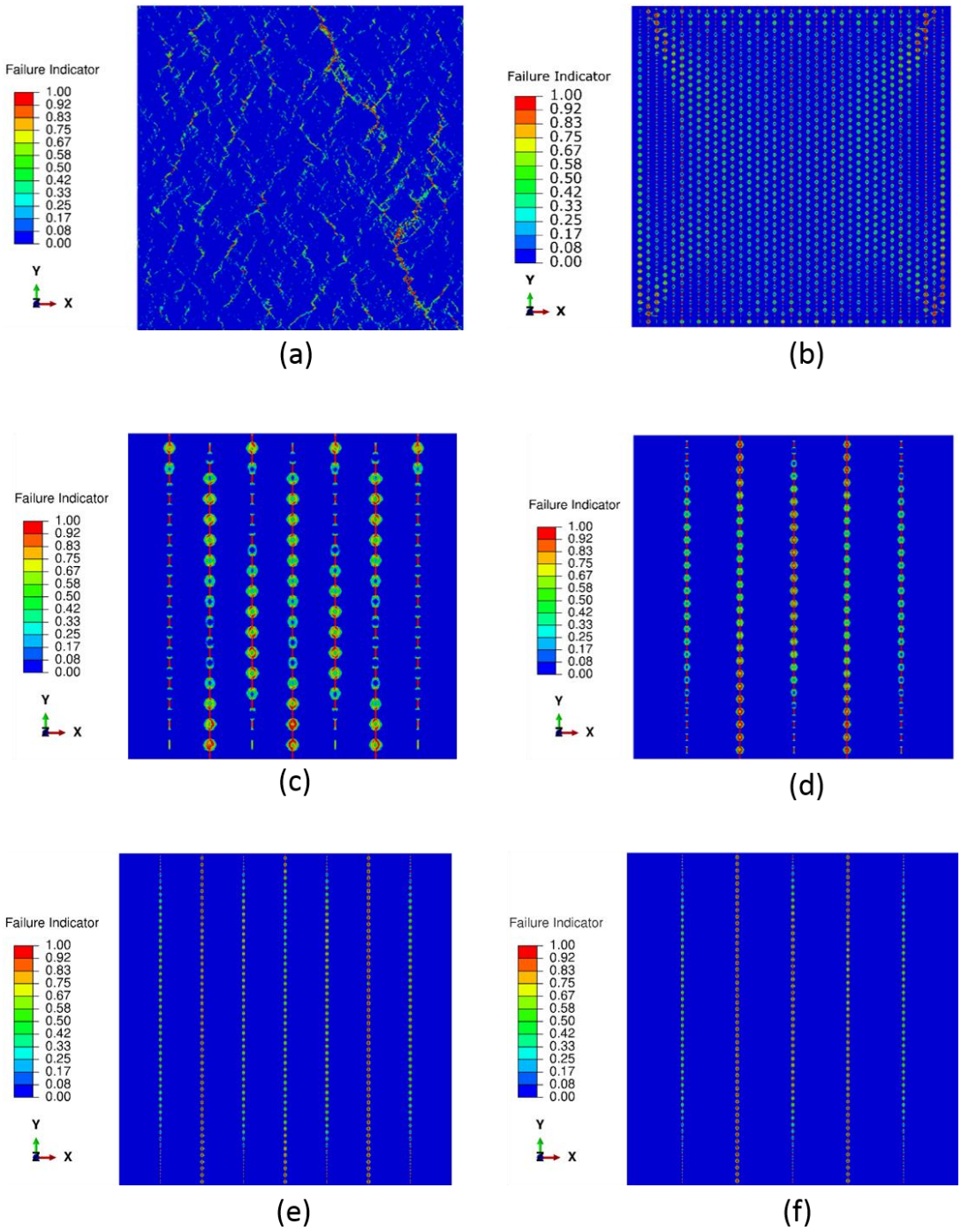

Figure 10. Predicted damage distributions and fracture patterns at final failure for: (a) the baseline lamellar-like microstructure, (b) *L/H*=5 (c) *L/H*=10, (d) *L/H*=20, (e) *L/H*=30, and (f) *L/H*=40 BAM microstructures.

The equivalent Von Mises stress distributions in the BAMs with *L/H* = 5 and 40 presented in Figs 11a and 11b, respectively, for a magnified zone at a stage of loading prior to the W onset of

cracking, further elucidate the origin of damage and failure mechanisms. The applied strain at this stage is 0.08. The size of this zone from the respective BAMs is the same. The stress concentrations build up in all the Ni/Fe ligaments and expand from the junction locations to the W bricks. Under increasing loading, the Ni/Fe ligaments fail first and the stress concentrations continue to build up in the W bricks until the bricks break and the cracks propagate through them. Similar to the mechanisms observed for the baseline material discussed previously (Fig. 4), the DPT mechanism due to failure of Ni/Fe elements combined with the crack-penetration-in-W-phase mechanism has led to an increased strength for the BAM composite. Comparing Fig. 11a to Fig. 11b reveals that there are substantially more stress concentration sites in the *L/H*=5 BAM than in the *L/H*=40 BAM. These stress concentration sites in the *L/H*=5 BAM produces many microcracks that are distributed over the domain while more limited cracks and crack distribution occur in the *L/H*=40 domain. Compared to the baseline microstructure, the *L/H*=5 BAM also has many distributed microcracks but the regular lattice microstructure does not contain a weak path like that occurring in the baseline one that favors crack propagation along such a path. More cracks distributed over the domain have triggered crack interactions at advanced stages of loading, and the combined crack distribution/interaction effect has produced increased fracture energy leading to substantially increased fracture strain for *L/H*=5 case. The strength obtained in the *L/H=5* case is also significantly increased compared to the *L/H=10* case (Table 2).

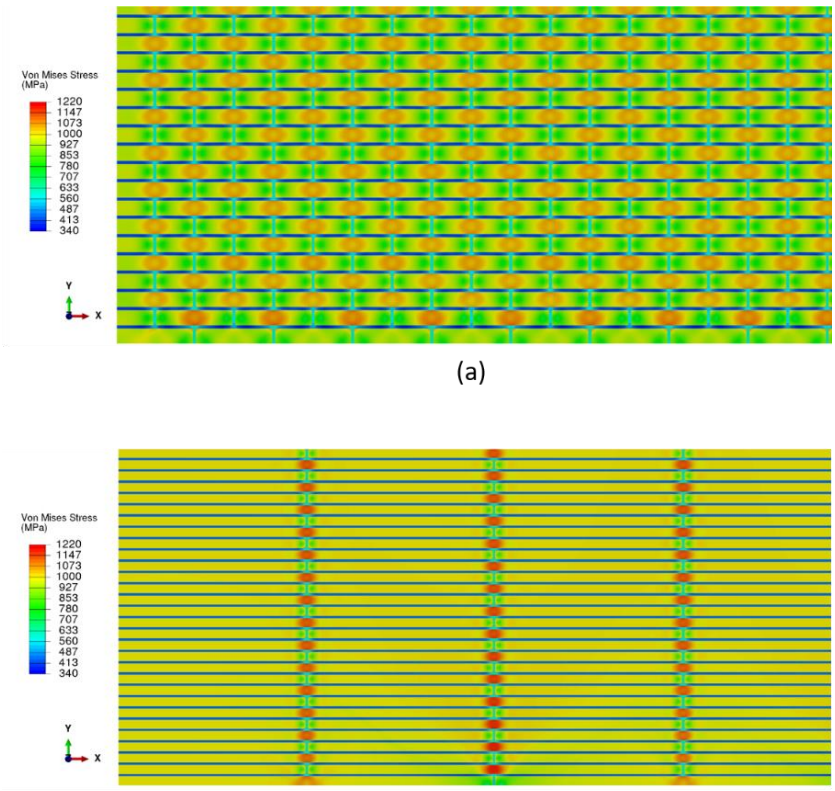

411

412 **Figure 11.** Magnified views of Von Mises stress distribution inside (a) *L/H*=5 BAM and (b)
413 *L/H*=40 BAM composites subject to tensile loading at 0.08 strain.

414 ## 4. Conclusions

415 We have applied a multiscale microstructural approach to simulate tensile loading of W-Ni/Fe
416 specimens cut out from a hot-rolled W-Ni/Fe composite with 0.8 W volume fraction. The predicted
417 material stress-strain response and crack patterns were then compared to the corresponding
418 experimental results to determine the elastic-plastic damage model parameters for W and Ni/Fe
419 phases in this domain. Subsequently, the model parameters were used to analyze W-Ni/Fe BAM
420 microstructures (arbitrarily designed) to investigate the effects of microstructural features on the
421 composite stress-strain response, strength, damage, and fracture patterns. The cracking and
422 fracture of the rolled W-Ni/Fe alloy (defined as the baseline material) appeared to be related to a
423 BAM microstructure consisting of weak but stiff bricks, or nearly brittle bricks, embedded in a
424 tough but less stiff mortar. We imagined building such a hierarchical microstructure using a simple
425 half-stagger BAM model. We were able to assign the W-bricks and Ni-Fe mortar in the BAM
426 microstructure the same constitutive properties as our baseline material using our developed FE

CDM model and the resulting stress-strain curves suggested that a finely divided but regular BAM microstructure was significantly better that our rolled W-Ni/Fe microstructure, but overall very similar. This type of correspondence needs to be further explored in the future but our model appears promising as a method to explore and optimize BAM architectures even though the FE discretization has some shortcomings in capturing some of the details of our rolled microstructure, such as unable to account for the weak W-W grain boundaries present in the rolled material.

The focus of this study is on tailoring the DPT W hierarchical microstructure to increase the resulting composite strength, ductility and fracture energy. Thus, the use of an elastic-plastic damage model with the rate-independent plasticity is justified for this purpose. However, other relevant types of constitutive behavior such as i.e., high-temperature and time-dependent behavior, irradiation hardening behavior, etc. can be modeled at the constituent phase level and incorporated in the developed multiscale modeling approach. For instance, the high-temperature response of the composite can be predicted by the same approach using the thermomechanical properties and stress-strain data at the corresponding high temperatures for the model parameter determination. In addition, thermal stresses due to the mismatch of coefficients of the thermal expansion between phases must be included in the constitutive equations. Regarding the application of this multiscale microstructural approach to high-temperature behaviors, the reader is referred to our previous work [14-15] in which it was applied to simulate microcracking of Ti_3SiC_2/SiC joints subjected to thermomechanical loading in addition to irradiation-induced swelling. To account for the loading rate effect, a rate-dependent plasticity constitutive model for the constituent phases must be used, and the model parameters should be determined for a given loading rate and then used to validate the model for other loading rates.

In this work, the model parameters have been determined from a hot-rolled W-Ni/Fe composite. Applying the developed multiscale approach to an unrolled W-Ni/Fe composite or a similar composite obtained under other rolling conditions (i.e., different rolling reduction ratios) requires the careful meshing of the as-formed microstructure (rolled or unrolled) by the same method described in Section 2.1 (see also Ref. [4]). Tensile stress-strain data obtained from unrolled or rolled materials from other rolling conditions should then be used to determine the model parameters since rolling conditions do have an important effect on the constituent phase material plasticity.

The following insights are drawn from this study:

- Different modeling scales from the micron scale of the constituent phases to a macroscale domain of a specimen are effectively bridged through the FE analysis that accounts for the constituent constitutive behavior.
- The microstructure study reveals the important effects of toughening mechanisms controlling the composite material mechanical properties that have been investigated in this work in terms of strength and failure strain. In addition to the DPT mechanism, crack penetrating into W phases combined with crack distribution and interaction over the domain can significantly contribute to the increased fracture energy, thus both increased strength and fracture strain for the composite.
- The predictive modeling tool has been applied to tailor the mechanical properties of W-BAM composites with the brick aspect ratio *L/H* as the selected design parameter under specific constraints on W volume fraction (0.8), the same dimension of the modeling domain, and regular lattice topology. Among the explored aspect ratios, BAM composite with $L/H = 5$ exhibits the most preferred combination of strength and fracture strain.
- The predictive modeling capability can be applied to explore additional material combinations, other microstructural topologies and parameters to determine optimal combinations of stiffness, strength, ductility and toughness for BAM composites.
- This capability can provide guidance to assist in processing BAM composites via a process such as e.g., 3D printing.

Our future work will include the application and extension of the developed approach to investigate W-composite high-temperature mechanical behaviors and irradiation effects.

5. Acknowledgements

This research was supported by U.S. Department of Energy (DOE), Office of Science, Office of Fusion Energy Sciences under Contract DE-AC05-76RL01830. PNNL is a multi-program national laboratory operated by Battelle Memorial Institute for the US DOE under DE-AC05-76RL01830.

6. References

[1] M. Rieth, J.L. Boutard, S.L. Dudarev, et al., Journal of Nuclear Materials 417 (2011) 463-467.

[2] R.A. Pitts, A. Kukushkin, A. Loarte, A. Martin, M. Merola, C.E. Kessel, V. Komarov, and M. Shimada, Physica Scripta (Volume T) T138 (2009) 014001 (10 pp.).

[3] P. Mertens, T. Hirai, M. Knaup, O. Neubauer, V. Philipps, J. Rapp, V. Riccardo, S. Sadakov, B. Schweer, A. Terra, I. Uytdenhouwen, U. Samm, Fusion Engineering and Design 84 (2009) (7-11) 1289-1293.

[4] B.N. Nguyen, C.H. Henager, Jr, N.R. Overman, R.J. Kurtz, Journal of Nuclear Materials 508 (2018) 371-384.

[5] M.E. Alam, G.R. Odette, Acta Materialia 186 (2020) 324-340.

[6] H. Gao, International Journal of Fracture 138 (2006) 101–137.

[7] K. Brandt, M.F.H. Wolff, V. Salikov, S. Heinrich, G.A. Schneider, Scientific Reports 3(2013): 2322 | DOI: 10.1038/srep02322.

[8] J. Henry, S. Pimenta, Journal of the Mechanics and Physics of Solids 118 (2018) 322–340.

[9] M.R. Begley, N.R. Philips, B.G. Compton, D.V. Wilbrink, R.O. Ritchie, M. Utz, Journal of the Mechanics and Physics of Solids 60(2012) 1545-1560.

[10] S. Pimenta, P. Robinson, Composites Science and Technology 104 (2014) 111–124.

[11] L. Gorbatikh, S.V. Lomov, I. Verpoest, Journal of the Mechanics and Physics of Solids 58 (2010) 735–750.

[12] K. Radi, D. Jauffrès, S. Deville, C.L. Martin, Journal of the Mechanics and Physics of Solids 126 (2019) 101–116.

[13] K. Radi, D. Jauffrès, S. Deville, C. L. Martin, Composites Part B 183 (2020) 107699.

[14] B. N. Nguyen, C.H. Henager Jr., R.J. Kurtz, Journal of Nuclear Materials 495 (2017) 504-515.

[15] B. N. Nguyen, C.H. Henager Jr., R.J. Kurtz, Journal of Nuclear Materials 499 (2018) 496-503.

[16] R. Neu, H. Maier, M. Balden, R. Dux, S. Elgeti, H. Gietl, H. Greuner, A. Herrmann, T. Höschen, M. Li, V. Rohde, D. Ruprecht, B. Sieglin and I. Zammuto, Journal of Nuclear Materials 511 (2018) 567-573.

[17] R. Neu, H. Maier, M. Balden et al., Fusion Engineering and Design 124 (2017) 450-454.

[18] Muyuan Li, D. Ruprecht, G. Kracker, T. Hoschen, R. Neu, Journal of Nuclear Materials 512 (2018) 1-7.

[19] S. Cierjacks, Fusion Engineering and Design 13 (1990) 229-238.

[20] S. J. Piet, E. T. Cheng, S. Fetter and J. S. Herring, Fusion Science and Technology 19 (1991) 146.

[21] S. Fetter, E. T. Cheng and F. M. Mann, Fusion Engineering and Design 6 (1988) 123-130.

[22] J. Lemaitre, in Continuum Damage Mechanics of Materials and Structures, O. Allix and F. Hild, Editors. 2002, Elsevier Science Ltd: Oxford, UK. p. 235-258.

[23] B.N. Nguyen, V. Kunc, International Journal of Damage Mechanics 19(6) (2010) 691-725.

[24] W Ramberg, WR Osgood. Description of stress–strain curves by three parameters. *Technical Note No. 902*, 1943, National Advisory Committee for Aeronautics, Washington DC.

[25] J. Lemaître, J.-L. Chaboche, Mécanique des Matériaux Solides. 1985, Paris, France: Dunod.

[26] V. Tvergaard, Journal of the Mechanics and Physics of Solids 30(6) (1982) 399-425.

[27] J.D. Eshelby, Proceedings of the Royal Society London, Series A (Mathematical and Physical Sciences). 252 (1959) 561-569.

[28] T. Mori, K. Tanaka, Acta Metallurgica 21 (1973) 571-4.

[29] Y. Benveniste, Mechanics of Materials 6 (1987) 147-57.